EHP Environmental Health Perspectives

pubs.acs.org/EnvHealthPerspectives
Article

Effects of Extreme Heat Exposure on Heatstroke and Liver Injury in Mice: The Role of PPARα

Guoqing Zhang, Lisha Zhao, Jiahui Wang, Kunyi Wang, Xiuyu Ji, Renjie Hu, Tong Hou, Lu Zhang, Ran Li, Qinghua Sun, Kezhong Zhang, and Cuiqing Liu*

Cite This: Environ. Health Perspect. 2026, 134, 110–123
Read Online

ABSTRACT: **BACKGROUND:** Liver injury is a frequent complication of heatstroke and constitutes a direct cause of death. However, only a few studies examined the mechanism underlying heatstroke-induced liver injury. **OBJECTIVE:** We aimed to evaluate the role of peroxisome proliferator-activated receptor α (PPARα) in heatstroke-induced liver injury and to explore the potential mechanisms. **METHODS:** Male C57BL/6N mice were subjected to a control (22 ± 1 °C) or extreme heat temperature (39.5 ± 0.5 °C) to induce a heatstroke-associated liver injury animal model. PPARα agonist, ferroptosis inhibitor, and AAV8-mediated PPARα overexpression were administered to the mice to investigate the role of PPARα and ferroptosis in the heatstroke-induced liver injury. Serum was collected for liver function evaluation. Liver tissues were applied for morphological observation, staining detection, ferroptosis examination, and mechanistic exploration. **RESULTS:** Compared with the control group, extreme heat exposure-induced temperature dysregulation, impaired liver function, and morphological damage in mice. Proteomics screened PPARα as a protein of interest, with its level being significantly decreased in response to extreme heat exposure. Both PPARα activation and overexpression attenuated extreme heat-induced heatstroke and liver injury. Hmox1 was next screened and higher Hmox1 expression was identified, accompanied by elevated markers of ferroptosis including prostaglandin-endoperoxide synthase 2 (Ptgs2), malondialdehyde (MDA), lipid peroxidation (LPO) and Fe^{2+} levels. Ferroptosis inhibition mitigated heatstroke and liver injury induced by heat exposure. In the setting of extreme heat exposure, PPARα activation suppressed Hmox1 expression and the levels of ferroptosis markers. It not only induced differences in the expression of members of iron generation, efflux and uptake process and reduced hepatic intracellular Fe^{2+} accumulation, but also stimulated expression of molecules for countering lipid peroxidation including Nrf2-SLC7A11-GPX4 axis and FSP1 signaling. **DISCUSSION:** PPARα played an essential role in extreme heat exposure-induced heatstroke and liver injury, and PPARα intervention conferred protection against it via inhibition of ferroptosis.

INTRODUCTION

Climate warming has been a serious problem and a growing issue, with the global mean surface temperature increasing by 0.61 °C from preindustrial era to period between 1986−2005, rising by 0.87 °C in the decade from 2006 to 2015,[1] and rising by 1.2 °C from the preindustrial era to 2020.[2] Global warming evokes enhanced frequency and intensity of extreme high temperature events, which pose detrimental health risks or even elevated mortality rates.[3,4] For instance, an exceptionally high temperature event in Russia during the summer of 2010 resulted in the deaths of approximately 55,000 people.[5] Similarly, a record-breaking extreme heat temperature event in Shanghai, China in 2013 resulted in 160 excess deaths in Pudong New District alone.[6] These phenomena indicate that global warming-induced extreme heat events have been a significant threat to global human health.

Heatstroke is the most severe disease derived from extreme heat exposure.[7] In response to extreme heat stress, the body's thermoregulatory capacity is exceeded, resulting in hyperthermia-induced damage and progressing to heatstroke. Elevated core temperatures (>40 °C), in conjunction with augmented oxidative stress following ischemia and blood redistribution, can instigate cellular, tissue or organ injury. The liver, heart, kidney, lung and brain are particularly susceptible organs.[3,8] Liver injury is a frequent complication of heatstroke and is the general and direct cause of death in patients suffering from heatstroke. Thus, in addition to the systemic supporting remedy, targeted therapy against liver injury should be the effective strategy for heatstroke-induced mortality.[9] To our knowledge, current evidence on the underlying mechanisms contributing to heatstroke-induced liver injury is limited to heat cytotoxicity and systemic inflammation due to impaired intestinal mucosal permeability which allows endotoxins to enter circulation.[9] Given the frequency and intensity of extreme heat temperature events, further mechanistic exploration is necessary and urgent for the development of effective intervention strategies.

Peroxisome proliferator-activated receptor α (PPARα), which is highly expressed in the liver, exerted transcriptional

Accepted: May 15, 2025
Published: April 23, 2026

https://doi.org/10.1021/EHP.6c00267
Environ. Health Perspect. 2026, 134, 110–123

regulation on a diverse array of molecules involved in metabolism (glucose, lipid and bile acid metabolism) and various metabolic pathways.[10,11] Interventions targeting PPARα-mediated regulation on metabolic disorders in hepatocytes have been shown to significantly attenuate liver injury in patients with sepsis.[12] Based on the shared pathophysiological process of lipid disorder in both heatstroke and sepsis,[13] there is the intriguing possibility that interventions aimed at PPARα may be capable of ameliorating heatstroke-induced liver injury.

Ferroptosis is a novel identified form of regulated cell death characterized by the iron-dependent accumulation of lipid peroxidation products, such as malondialdehyde (MDA).[14] It was derived from iron metabolism disorder and disruption of redox homeostasis, which led to the peroxidation of membrane phospholipids, membrane rupture, and ultimately cell death.[15] Hou et al. demonstrated that heat stress resulted in elevated levels of reactive oxygen species[16] and MDA, the product of lipid peroxidation, in rats.[16,17] However, whether and how ferroptosis is involved in the pathogenesis of heatstroke-induced liver injury remains undetermined.

In this study, we attempted to explore the molecular mechanisms underlying extreme heat-induced liver injury by screening and particularly focusing on PPARα-mediated ferroptosis as well as the therapeutic strategies by conducting pharmacological PPARα activation and liver-specific PPARα overexpression.

MATERIALS AND METHODS

1.1. Animal Care and Use

Given the sex-related differences in thermoregulation in mice, we chose to focus on male subjects, which are more responsive to temperature variations.[18] C57BL/6N male mice (7−8 weeks old) were purchased from Charles River Laboratories (Beijing, China). All mice were housed under standard laboratory conditions (22 ± 1 °C, 12 h light/dark cycle) with *ad libitum* access to water and food (Xietong Organism, Nanjing, China). All animal experiments were approved by the Institutional Animal Care and Use Committee at Zhejiang Chinese Medical University under protocol 13294.

1.2. Murine Model of Heat Stroke

Following 1 week of acclimatization feeding, C57BL/6N mice (n = 10 per group) were randomly assigned to the control group (22 ± 1 °C) or extreme heat group (39.5 ± 0.5 °C) using the Zhejiang Whole-body Exposure System (ZJ-WES, Zhejiang Qiushi Artificial Environment Co., Ltd.).[19] The ZJ-WES with an internal volume of 130 cm (width) × 65 cm (depth) × 180 cm (height). The heat within the chamber is generated via a built-in heating element, and the temperature was precisely controlled by using a compressor-based temperature regulation mechanism. A temperature sensor within the system continuously monitored the internal temperature, providing feedback for accurate temperature maintenance. Mice were housed by one animal per cage, being deprived of water and food during heat exposure. Core body temperature (Tc) was monitored using a thermocouple (BW-TH1101, Shanghai, China). Heatstroke onset was defined as the point at which Tc reached a maximum (Tc,max) with no further increase in Tc during the temperature measurements or the mouse exhibited signs of heat exhaustion as described in previous study.[20] Heat exhaustion was characterized by behavioral changes such as sluggishness, unresponsiveness, and a loss of grip strength. Then mice were removed from the whole-body exposure chamber, weighed, and transferred to the control environment (22 ± 1 °C) with *ad libitum* access to water and food. Tc was monitored during the recovery period, and Tc,min was identified until it reached the nadir with no further decrease in Tc. Mice were euthanized at Tc,min, also known as the hyperthermia depth (HS-HD), or after 9 h of recovery (HS-9h).

1.3. Construction of Mouse Model with Liver-Specific PPARα Overexpression and Heat Exposure

The AAV8 delivery system that overexpresses the PPARα gene in mouse livers was constructed by Rongsen Gene Technology Co., Ltd. (Jiangsu, China). The empty associated adenovirus (AAV8-null) served as a control. Titers of the vector genome were measured by quantitative qRT-PCR with vector-specific primers. The 5- to 6-week-old male C57BL/6N mice were injected with 150 μL of virus containing 5×10^{12} AAV8 vector genomes via the tail vein. Three weeks later, the efficiency of hepatic PPARα overexpression in the liver was verified with Western blot.

To investigate the role of hepatic PPARα overexpression in heat-induced injury, mice expressing either AAV8-null (control) or AAV8-PPARα (hepatic PPARα overexpression) were subjected to either control or extreme heat conditions. Mice were randomly assigned to one of four groups (n = 10 per group): control (AAV8-C), hepatic PPARα overexpression (AAV8-P), extreme heat (AAV8-H), and extreme heat with hepatic PPARα overexpression (AAV8-HP). After heatstroke onset, mice were moved to control environment (22 ± 1 °C) for a 9 h recovery period.

1.4. Preventive Administration of PPARα Agonist and Ferroptosis Inhibitor

For preventive intervention of PPARα activation, mice were gavaged with either PPARα agonist fenofibrate (FF, 200 mg/kg body weight; Sigma) or vehicle (ddH_2O containing 1% carboxymethylcellulose sodium; CMC-Na) 20 and 4 h prior to exposure to extreme heat. The dose was chosen based on previous study.[21] The mice were randomly divided into four groups (n = 10 per group): control group (CC), control group treated with FF (CF), extreme heat group (HC), and extreme heat group treated with FF (HF). After heatstroke onset, mice were moved to control environment (22 ± 1 °C) for a 9 h recovery period.

For preventive intervention of ferroptosis inhibition, mice were intraperitoneally injected with either ferroptosis inhibitor ferrostatin-1 (Fer-1, 10 mg/kg body weight; Selleck Chemicals) or vehicle (ddH_2O containing 5% DMSO + 40% PEG 300 + 5% TWEEN 80) 1 h prior to exposure to extreme heat. The dose was chosen based on previous study.[20] The mice were randomly divided into four groups (n = 10 per group): control group (CC), control group treated with FF (CFer-1), extreme heat group (HC), and extreme heat group treated with FF (HFer-1). After heatstroke onset, mice were moved to control environment (22 ± 1 °C) for a 9 h recovery period.

1.5. Therapeutic Administration of PPARα Agonist and Ferroptosis Inhibitor

For therapeutic intervention of PPARα activation, mice were administered either FF (250 mg/kg body weight; Sigma) or vehicle control (ddH_2O containing 1% carboxymethylcellulose sodium; CMC-Na) via oral gavage immediately at the onset of heatstroke. Sixteen hours later, the same dose of FF or vehicle was administered again. The dose was chosen based on preliminary experiments. The mice were randomly divided into four groups (n = 10 per group): control group (T-CC), control group treated with FF (T-CF), extreme heat group (T-HC), and extreme heat group treated with FF (T-HF). After heatstroke onset, mice were moved to control environment (22 ± 1 °C) for a 24 h recovery period. The dose of FF was chosen based on preliminary observations.

For therapeutic intervention of ferroptosis inhibition, mice received either the Fer-1 (7 mg/kg body weight; Selleck Chemicals) via intraperitoneal injection or vehicle control (ddH_2O containing 5% DMSO + 40% PEG 300 + 5% TWEEN 80) at the onset of heatstroke, followed by a second injection of the same dose of Fer-1 or vehicle 12 h later. The dose was chosen based on preliminary experiments. The mice were randomly divided into four groups (n = 10 per group): control group (T-CC), control group treated with FF (T-CFer-1), extreme heat group (T-HC), and extreme heat group treated with FF (T-HFer-1). After heatstroke onset, mice were moved to control

https://doi.org/10.1021/EHP.6c00267
Environ. Health Perspect. 2026, 134, 110−123

environment (22 ± 1 °C) for a 24 h recovery period. The dose of Fer-1 was chosen based on preliminary observations.

1.6. Sample Collection

At the end of the experiment, the mice were euthanized with isoflurane, and blood was collected via enucleation. Serum was obtained by allowing the blood to clot at room temperature for 30 min, followed by centrifugation at 2,000 relative centrifugal force (rcf) for 10 min at 4 °C. Serum samples were stored at −80 °C. In order to minimize the error due to sample collection, liver was harvested and weighed, and the left lobe was divided to allow for distinct processing methods. One portion was immediately snap-frozen in liquid nitrogen, while the other portion was fixed in 4% paraformaldehyde (Yuanye Bio-Technology, Shanghai, China) for further analysis.

1.7. Plasma Measurements

The serum was analyzed for alanine aminotransferase (ALT, Medicalsystem Biotech., Ningbo, China) and aspartate aminotransferase (AST, Medicalsystem Biotech., Ningbo, China) levels using a Cobas c-111 biochemistry analyzer (Roche Diagnostics).

1.8. Histological Analysis and Quantification of Liver Tissue

Liver tissues from mice were fixed in 4% paraformaldehyde for 24 h and then dehydrated and embedded in paraffin. The embedded tissues were then sectioned into 5 μm thick slices using a rotary microtome (HM325, Thermo Fisher, UK) and placed on glass slides. After deparaffinization and rehydration, liver sections were stained with hematoxylin and eosin (H&E). The severity of liver injury was assessed and graded according to Suzuki's criteria on a scale of 0 to 4. No necrosis, congestion, or centrilobular ballooning is given a score of 0, while severe congestion and greater than 60% lobular necrosis is given a value of 4 (n = 5 per group).

1.9. Proteomics

Proteomics was constructed by Shanghai Applied Protein Technology Co., Ltd. (Shanghai, China). Briefly, Proteins were extracted from frozen liver tissues using SDT buffer (4% SDS, 100 mM Tris−HCl, 1 mM DTT, pH 7.6). SDT buffer was added to the liver tissue samples, which were then homogenized. The homogenate was sonicated (2000 W, 30 s pulses with 30 s intervals for a total of 60 cycles). Following sonication, samples were heated in a boiling water bath for 8 min to denature the proteins. After heating, samples were centrifuged at 12,000g for 20 min at 4 °C, and the supernatant was collected and aliquoted for subsequent protein quantification. Concentrations were quantified with BCA protein assay (#P0012, Beyotime, China), and 20 μg of protein for each sample were mixed with 5× loading buffer respectively and boiled for 5 min. The proteins were separated on a 12.5% SDS-PAGE gel (constant current 14 mA, 90 min). Protein bands were visualized by Coomassie Blue R-250 staining to assess the quality. Protein digestion by trypsin was performed according to filter-aided sample preparation (FASP) procedure: 200 μg of proteins for each sample were incorporated into 30 μL of SDT buffer (4% SDS, 100 mM DTT, 150 mM Tris−HCl pH 8.0). The detergent, DTT (#161-0404, Bio-Rad, USA) and other low-molecular-weight components were removed using UA buffer (8 M Urea, 150 mM Tris−HCl pH 8.0) by repeated ultrafiltration (Microcon units, 10 kDa). Then 100 μL of iodoacetamide (100 mM IAA in UA buffer) was added to block reduced cysteine residues, and the samples were incubated for 30 min in darkness. The filters were washed with 100 μL of UA buffer three times and then 100 μL of 25 mM NH_4HCO_3 buffer twice. Finally, the protein suspensions were digested with 4 μg of trypsin in 40 μL of 25 mM NH_4HCO_3 buffer overnight at 37 °C, and the resulting peptides were collected as a filtrate. The peptides of each sample were desalted on C18 cartridges (#6687-U, Sigma, USA), concentrated by vacuum centrifugation (2000 rpm for 3 h at −60 °C) and reconstituted in 40 μL of 0.1% (v/v) formic acid. The peptide content was estimated by UV light spectral density at 280 nm using an extinctions coefficient of 1.1 of 0.1% (g/L) solution that was calculated on the basis of the frequency of tryptophan and tyrosine in vertebrate proteins. The digest peptides of each sample were desalted on C18 cartridges, concentrated by vacuum centrifugation and reconstituted in 40 μL of 0.1% (v/v) formic acid. Digested peptide samples (100 μg) were labeled with tandem mass tag (TMT) regent (#A40000839, Thermo Fisher Scientific, USA). Next, labeled peptides were fractionated using strong cation exchange (SCX) chromatography on an AKTA Purifier system (#23628, GE Healthcare, USA). Liquid chromatography/mass spectrometry liquid chromatography−mass spectrometry/mass spectrometry (LC-MS/MS, Q Exactive HF-X, Thermo Scientific) was used to measure TMT-labeled peptides. The raw data from the MS were analyzed using the MASCOT search engine (Matrix Science, London, UK; version 2.2), which is embedded in the Proteome Discoverer 1.4 software package, to identify and quantify proteins.

1.10. Protein−Protein Interaction (PPI) Analysis

Differentially expressed proteins, both up- and down-regulated, are typically included in screenings from proteomics data. Protein identifiers are converted into a format recognized by the STRING database. Using the STRING database (https://string-db.org/), a PPI network is generated and subsequently exported. These data are then imported into Cytoscape (version 3.10.1) for visualization and analysis. Differentially expressed proteins are sorted by their degree (number of interactions) to allow for the identification of hub proteins, which are considered to be central to the network. Finally, the PPI network is visualized in Cytoscape with core proteins highlighted.

1.11. Quantitative RT-PCR

Total RNA was extracted from frozen liver tissue with RNAiso Plus (Takara Biotechnology, Dalian, China). The RNA concentrations were measured using a NanoDrop2000 ultra microspectrophotometer (Thermo Fisher Scientific, Waltham, USA), and the absorbance ratio at 260/280 nm was between 1.8 and 2.0 to ensure RNA quality purity. Then the RNA was reverse transcribed into complementary DNA (cDNA) using the PrimeScript RT Master Mix (Takara Biotechnology, Dalian, China). mRNA expression was quantified using the Quant-Studio Q7 system (Applied Biosystems, Carlsbad, CA, USA) with the following cycling program: 50 °C for 2 min, 95 °C for 2 min (activation), 40 cycles of 95 °C for 15 s (denaturation), and 60 °C for 1 min (extension). All data were normalized to the expression of the housekeeping gene β-actin (n = 8 per group). The primer sequences used for PCR are given in Table S1. The primers were synthesized by Tsingke Biotechnology (Hangzhou, China).

1.12. Western Blot Analysis

Frozen liver tissue was homogenized in radio-immunoprecipitation assay (RIPA) buffer (Boster Biological Technology Co. Ltd., CA, USA) supplemented with phosphatase and protease inhibitors using a grinder and then incubated on ice for 30 min with periodic vortexing and centrifuged (12,000 g for 15 min at 4 °C). The resulting supernatant was collected as a protein solution. Concentrations were quantified with a BCA protein assay (#5000001, BIO-RAD, California, USA). Equal amounts of liver protein (5−10 mg) were analyzed by 10% sodium dodecyl sulfate-polyacrylamide gel electrophoresis (SDS-PAGE) and transferred to polyvinylidene fluoride (PVDF) membranes, which were blocked with 5% skim milk for 1 h and incubated with following primary antibodies overnight at 4 °C:heme oxygenase 1 (Hmox1, #82206s, 1:1000), nuclear factor erythroid 2-related factor 2 (Nrf2, #12721, 1:1000), β-actin (#4970, 1:5000) from Cell Signaling Technology (Danvers, MA, USA); glutathione peroxidase 4 (GPX4, #ab125066, 1:1000) from abcam (Cambridge, UK); ferroportin (FPN, #NBP1-21502, 1:1000) from Novus Biologicals (Littleton, Colorado, USA); ferroptosis suppressor protein 1 (FSP1, #20886-1-AP, 1:1000) from Proteintech (Wuhan, China); solute carrier family 7, Member 11 (SLC7A11, #A2413, 1:1000) from ABclonal (Wuhan, China); and PPARα (#sc-398394, 1:1000) from Santa Cruz Biotechnology (Dallas, Texas, USA). The PVDF membranes were then visualized using HRP enzyme-labeled secondary antibody (Multi Sciences, #GAM0072, 1:5000; Proteintech, #SA00001, 1:5000). Images were acquired using a ChemiDoc Imaging System (Bio-Rad, California, USA), and semiquantitative

https://doi.org/10.1021/EHP.6c00267
Environ. Health Perspect. 2026, 134, 110−123

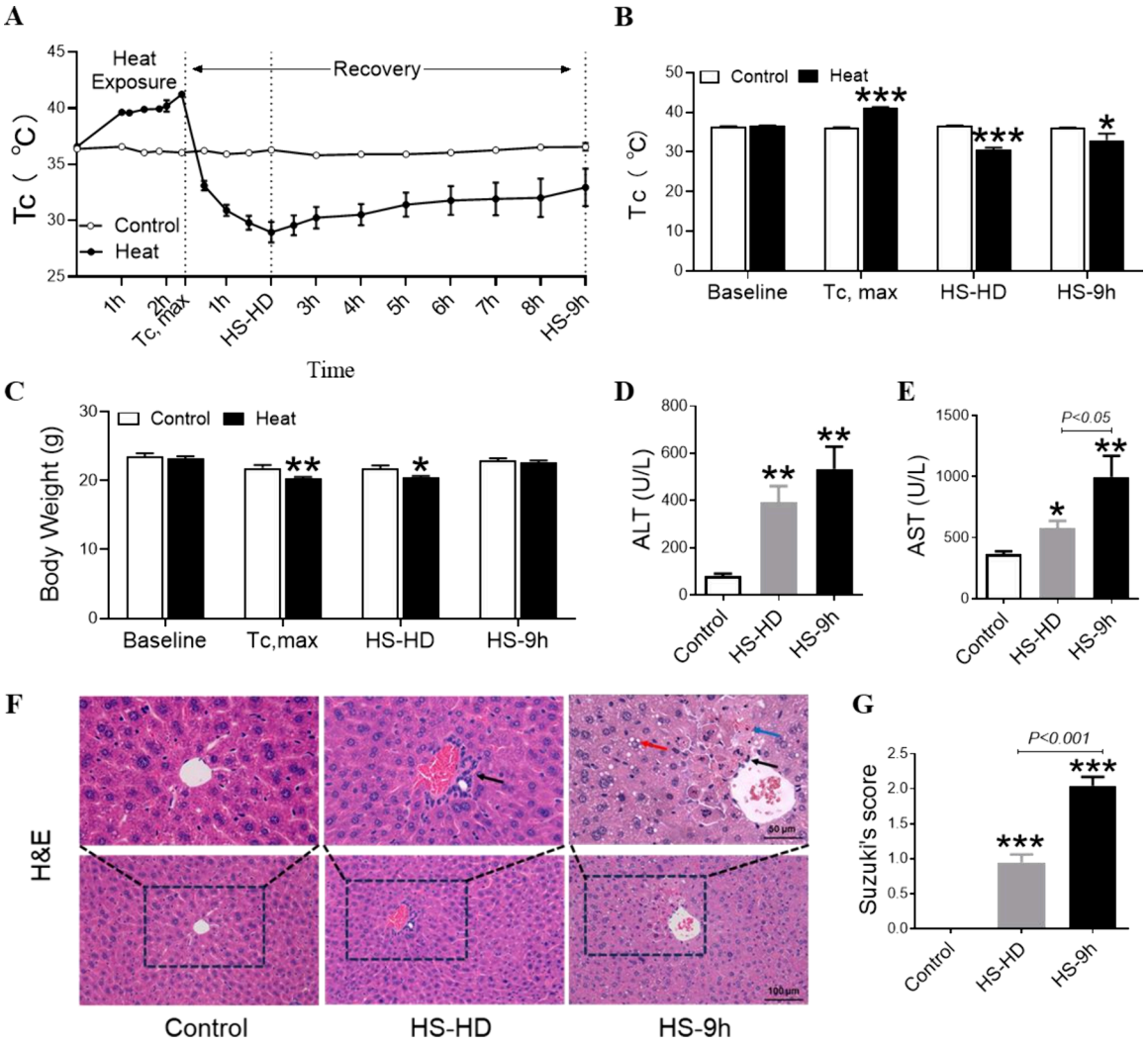

Figure 1. Effects of extreme heat exposure on Tc and the liver in murine models. Mice were exposed to extreme heat until heatstroke onset and then allowed to recover at 22 °C until HS-HD and HS-9h. A, The Tc of mice during heat exposure and recovery period (n = 8). B, Tc at baseline, Tc,max, HS-HD and HS-9h (n = 8). C, Body weight at baseline, Tc,max, HS-HD and HS-9h (n = 8). D,E, Serum ALT (D) and AST (E) levels at HS-HD and HS-9h (n = 8). F,G, Representative images (F) and Suzuki's score (G) of H&E-stained liver sections (black arrows indicate inflammatory infiltrates; red arrows indicate vacuole-like changes; blue arrows indicate congestion) (n = 5). The numeric data are shown in Table S2. Data are presented as means ± SEM and assessed through t-test or one-way ANOVA. *p < 0.05, **p < 0.01, ***p < 0.001 when compared with control group. Note: Tc, core body temperature; HS, heatstroke; HD, hyperthermia depth; H&E, hematoxylin−eosin; ALT, alanine aminotransferase; AST, aspartate aminotransferase; SEM, standard error of the mean; ANOVA, analysis of variance.

analysis was performed using ImageJ software (version 1.8.0) (n = 4 per group).

1.13. Total Iron Level

The total iron content of liver tissues was determined using a total iron content assay kit (no. A039, Jiancheng, Nanjing, China) which included the following solutions for analysis. Briefly, 50 mg of frozen liver tissue was homogenized with an automatic grinder in physiological saline and centrifuged (2500 rpm for 10 min at 4 °C). The supernatant was collected and used to measure the protein concentration. Another aliquot of the supernatant was used for the iron assay. A blank and standard tubes were set up in parallel. 600 μL of iron stain was then added to the supernatant, blank, and standard tubes (200 μL). After mixing, the tubes were incubated in a water bath at 100 °C for 5 min. After incubation, the tubes were cooled and centrifuged (3500 rpm for 10 min at room temperature). Transfer 200 μL of the supernatant to a 96-well plate and measure the absorbance at 520 nm using a microplate reader (#SpectraMax M3, Bio Tek, USA).

1.14. Fe^{2+} Level

The Fe^{2+} content of liver tissues was determined using a Fe^{2+} assay kit (#ab83366, Abcam, Cambridge, UK) which included the following solutions for analysis. In brief, 50 mg of frozen liver tissue was homogenized with a cryogenic grinder in Iron Assay Buffer and subsequently centrifuged at 16000g for 10 min at 4 °C. The supernatant was collected and used for further analysis. The samples and standard solutions were added to a 96 well plate, and then 5 μL of iron assay buffer and 5 μL of iron reducer were added to each well. After mixing, the plate was incubated at 37 °C for 30 min. 100 μL of iron probe was then added to each well, and the plate was incubated at 37 °C for 60 min. Finally, the absorbance at 593 nm of the sample and standard solutions was measured using a microplate reader (SpectraMax M3, Bio Tek, USA).

1.15. Malondialdehyde (MDA) Level

The MDA level of liver tissues was determined using an MDA assay kit (no. A003, Jiancheng, Nanjing, China) which included the following solutions for analysis. In brief, 50 mg of frozen liver tissue was homogenized with a cryogenic grinder in saline solution and

https://doi.org/10.1021/EHP.6c00267
Environ. Health Perspect. 2026, 134, 110−123

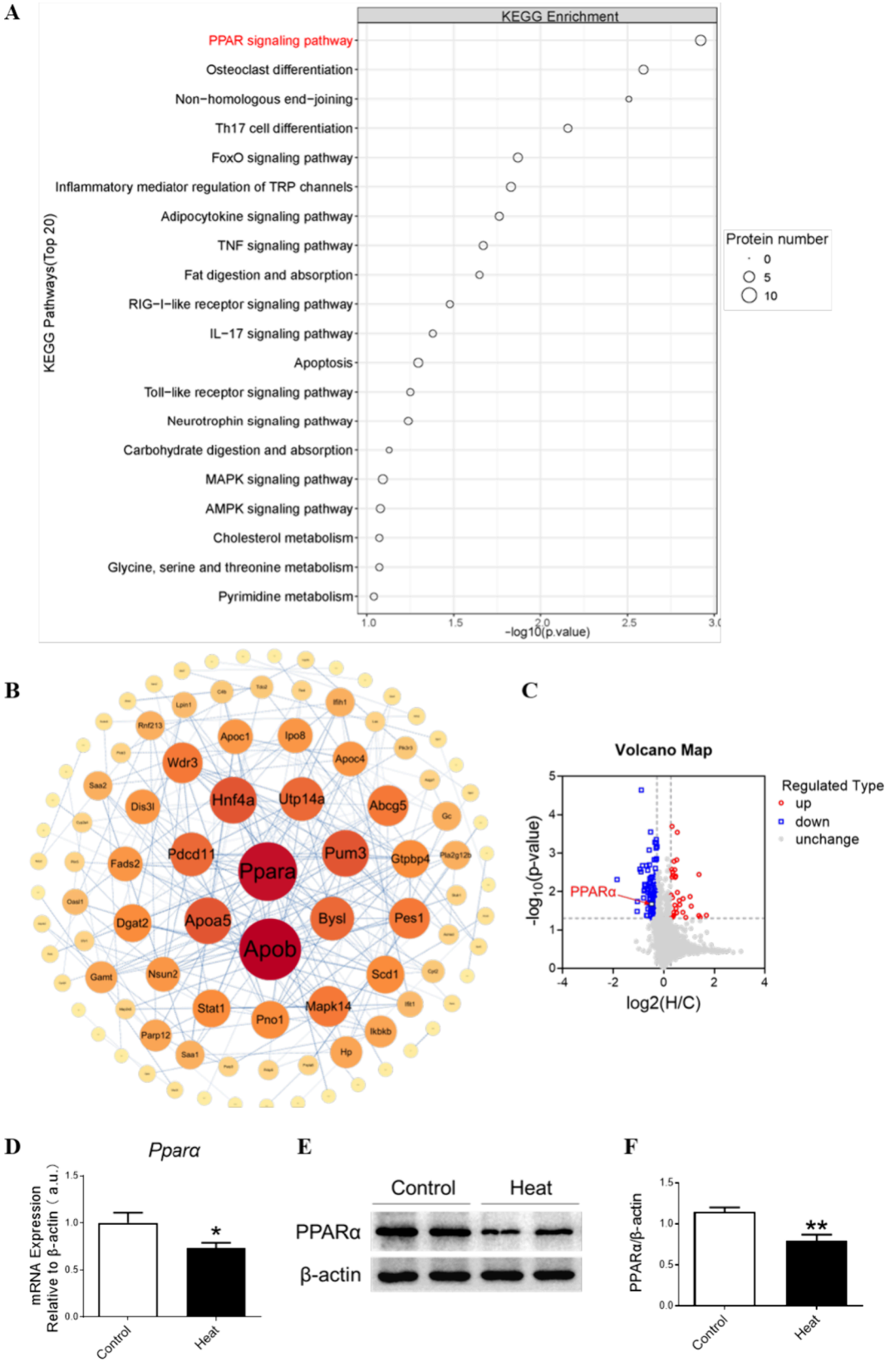

Figure 2. PPARα levels in the liver of mice exposed to extreme heat. Mice were exposed to extreme heat until heatstroke onset and then allowed to recover at 22 °C for 9 h. A, KEGG signaling pathway analysis of proteomics with liver tissue (n = 3). B, Core protein network analysis of proteomics with liver tissue (n = 3). C, Volcano plot of proteomics with liver tissue (n = 3). D, The mRNA levels of *Pparα* in the liver (n = 8). E,F, Representative bands (E) and analyzed protein levels of PPARα (F) in the liver (n = 4). The numeric data are shown in Table S3. Data are presented as means ± SEM and assessed through t-test. *p < 0.05, **p < 0.01 when compared with control group. Note: PPARα, peroxisome proliferator-activated receptor α; KEGG: kyoto encyclopedia of genes and genomes; SEM, standard error of the mean.

https://doi.org/10.1021/EHP.6c00267
Environ. Health Perspect. 2026, 134, 110−123

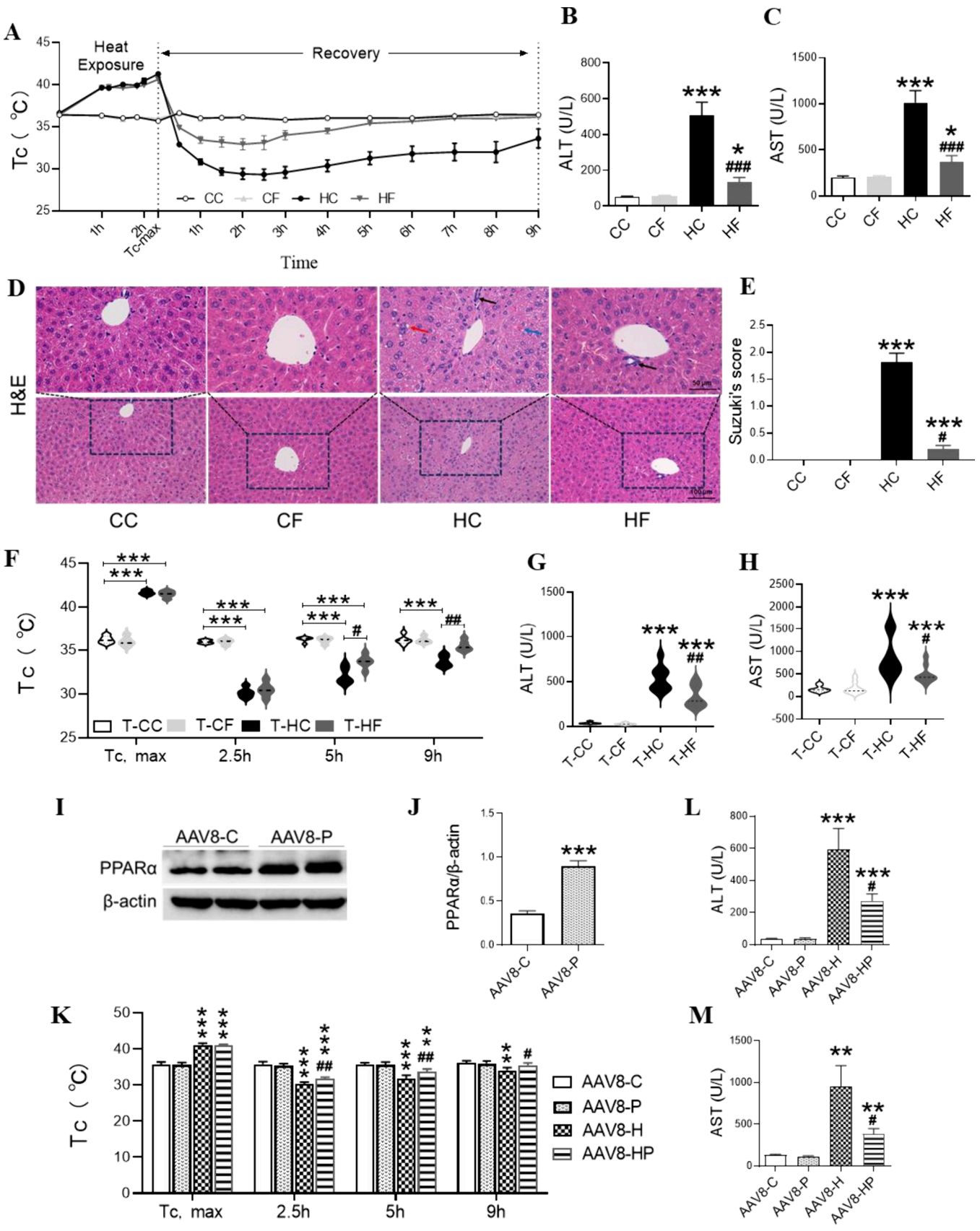

Figure 3. Effects of PPARα intervention on Tc dysregulation and liver injury in mice exposed to extreme heat. (A−H) Mice were treated with the PPARα agonist fenofibrate before/after heatstroke induction, followed by either a 9 h or 24 h recovery period at 22 °C. A, The Tc of mice during heat exposure and recovery period in the mice with FF preadministration (n = 8). B,C, Serum ALT (B) and AST (C) levels at HS-9h (n = 8). D,E, Representative images (D) and Suzuki's score (E) of H&E-stained liver sections. (black arrows indicate inflammatory infiltrates; red arrows indicate vacuole-like changes; blue arrows indicate congestion) (n = 5). F, The Tc at the onset of heatstroke and during recovery period in the mice with FF

https://doi.org/10.1021/EHP.6c00267
Environ. Health Perspect. 2026, 134, 110−123

Figure 3. continued

therapeutic administration (n = 8). G,H, Serum ALT (G) and AST (H) levels at HS-24h (n = 8). (I−M) Mice expressing control (AAV8-null) or PPARα-overexpressing (AAV8-PPARα) vectors were exposed to extreme heat until heatstroke onset and then allowed to recover at 22 °C for 9 h. I,J, Representative bands (I) and analyzed protein levels of PPARα (J) in the liver-specific PPARα overexpressed mice (n = 4). K, The Tc of mice at the onset of heatstroke and during recovery period in the liver-specific PPARα overexpressed mice (n = 8). L,M, Serum ALT (L) and AST (M) levels at HS-9h (n = 8). The numeric data are shown in Table S4. Data are presented as means ± SEM and assessed through t-test or two-way ANOVA. $^{*}p < 0.05$, $^{***}p < 0.001$, compared with CC group; $^{\#\#}p < 0.01$, $^{\#\#\#}p < 0.001$, compared with heat group. Note: PPARα, peroxisome proliferator-activated receptor α; HS, heatstroke; ALT, alanine aminotransferase; AST, aspartate aminotransferase; H&E, hematoxylin and eosin; SEM, standard error of the mean; ANOVA, analysis of variance.

centrifuged at 2500 rpm for 10 min at 4 °C. The supernatant was collected to measure protein concentration and MDA levels. A blank, control, and standard tubes were set up in parallel. Blank, standard, and sample tubes (100 μL) were each added with reagent 2 (900 μL) and reagent 3 (100 μL), while control tubes were added with reagent 2 (900 μL) and 50% glacial acetic acid (100 μL). After mixing, the tubes were incubated at 95 °C for 40 min. After cooling and centrifugation (4000 rpm for 10 min at room temperature), 200 μL of supernatant was added to the 96 well plate. Finally, the absorbance at 532 nm of the sample, blank, control, and standard solutions was measured using a microplate reader (#SpectraMax M3, Bio Tek, USA).

1.16. Lipid Peroxidation (LPO) Level

LPO level in liver tissues was determined using an LPO assay kit (#A106, Jiancheng, Nanjing, China) which included the following solutions for analysis. Briefly, 50 mg of frozen liver tissue was homogenized with a cryogenic grinder in saline solution and centrifuged at 2500 rpm for 10 min at 4 °C. The supernatant was collected to measure protein concentration and LPO levels. Blank and standard tubes were set up in parallel. Reagent 1 (650 μL) and reagent 2 (150 μL) were added to the blank, standard, and sample tubes (200 μL) in that order and mixed well. Then the tubes were incubated at 45 °C for 60 min. After centrifugation (4000 rpm for 10 min at room temperature), 200 μL of supernatant was added to the 96 well plate. Finally, the absorbance at 586 nm of the sample, blank, and control standard solutions was measured using a microplate reader (#SpectraMax M3, Bio Tek, USA).

1.17. C11 BODIPY Staining

Lipid peroxidation was assessed using the C11-BODIPY 581/591 fluorescent probe (no. D3861, Invitrogen, California, USA) following the manufacturer's protocol. Briefly, frozen tissue sections mounted on glass coverslips were incubated in the dark for 30 min at 37 °C with 1 μM C11-BODIPY 581/591. Sections were then rinsed with PBS, fixed in 4% paraformaldehyde at room temperature for 20 min, and washed three times with PBS. Slides were mounted with DAPI. Oxidized (green) and nonoxidized (red) lipid signals were detected using 488/510 nm (FITC) and 581/591 nm (Texas Red) filters, respectively, and imaged with a Leica Upright Epifluorescence Microscope (DM6, Wetzlar, Germany). Three random fields of view per sample were captured. ImageJ software (version 1.8.0) was used for semiquantitative image analysis.

1.18. Transmission Electron Microscope (TEM)

Mice were anesthetized and perfused with phosphate-buffered solution. Tiny amount of liver tissues (<1 mm^3) was then dissected and fixed overnight at 4 °C in a 2.5% glutaraldehyde solution. After rinsing twice in 0.1 M PB solution and twice in ddH_2O (10 min each), the tissue was postfixed in a 1% osmic acid plus 1.5% potassium ferricyanide mixture for 1 h at 4 °C, followed by ddH_2O washes for four times (10 min each). The tissue was then treated with TCH for 1 h at room temperature, rinsed four times in ddH_2O (10 min each), and postfixed again in 1% osmic acid for 1 h at 4 °C, followed by three ddH_2O washes (10 min each). After an overnight fixation in 2% uranyl acetate at 4 °C and three ddH_2O washes (10 min each), the tissue was dehydrated in a graded ethanol series (50% to 100%, 10 min each) and washed twice in 100% acetone (10 min each). The tissue was then infiltrated with a 1:1 acetone:embedding resin mixture for 1 h, followed by a 1:3 mixture overnight, and finally embedded in pure resin with two changes (8 h and overnight). The samples were polymerized at 60 °C, sectioned (70 nm), and double-stained with uranyl acetate and lead citrate. The mitochondrial morphology was visualized by transmission electron microscopy (HT7700, HITACHI, Japan).

1.19. Co-immunoprecipitation (Co-IP)

Frozen liver tissues were lysed with Lysis Buffer, and lysates were centrifuged at 12,000g for 5 min at 4 °C. Precleared protein extracts were incubated with anti-PPARα antibody (66826-1-Ig, 2 μg/mL, Proteintech) or normal IgG (12−371B, Millipore, New Bedford, USA) at 4 °C overnight, followed by the incubation with Protein A/Gc beads (#88802, Thermo Fisher Scientific, Waltham, USA) at 4 °C for 4 h. The protein complexes were then washed and subjected to Western blot analysis to detect the levels of PPARα (#sc-398394, 1:1000, Santa Cruz) and Hmox1 (no. 82206s, 1:1000, CST). Whole cell lysates served as an input control, and normal IgG acted as a negative control. The PVDF membranes were visualized using HRP-conjugated Goat Anti-Mouse IgG Light Chain (Abclonal, #AS062, 1:5000) and HRP-conjugated Goat Anti-Rabbit IgG Heavy Chain (Abclonal, #AS063, 1:5000). Images were acquired using a ChemiDoc Imaging System (Bio-Rad, California, USA).

1.20. Data Analysis

Data were expressed as means ± the standard error of the mean (SEM). Statistical evaluation was performed by unpaired two-tailed Student's t test, one-way or two-way analysis of variance (ANOVA) using GraphPad Prism version 8.0, and Tukey's test was used as a post hoc test. $p < 0.05$ was considered statistically significant.

RESULTS

Liver Injury in Mice Exposed to Extreme Heat

To explore the effects of liver function following an extreme heat challenge, we established a murine heatstroke model with high incidence of liver injury. As shown in Figure 1A, the Tc of mice continuously rose during heat exposure. At the onset of heatstroke, mice were removed to a control environment (22 ± 1 °C) for recovery. We observed that the Tc began to drop sharply until to the nadir (HS-HD) and then rise gradually. At 9 h postheatstroke (HS-9h), the Tc of mice in the extreme heat exposure group was still significantly lower than control (Figure 1A,B). Concomitantly, a significant decrease in body weight at both Tc,max and HS-HD was noticed, which returned to normal at HS-9h (Figure 1C). Additionally, ALT (Figure 1D) and AST (Figure 1E) levels time-dependently increased in response to heat exposure, while liver weight and its organ coefficients at either HS-HD (Figure S1A,B) or HS-9h (Figure S1C,D) showed no significant alteration. Consistent with these findings, the most severe histological changes (Figure 1F) and Suzuki's score (Figure 1G) in the liver at HS-9h was observed, as evidenced by the markedly increased congestion, vacuole-like changes, and inflammatory infiltrates.

https://doi.org/10.1021/EHP.6c00267
Environ. Health Perspect. 2026, 134, 110−123

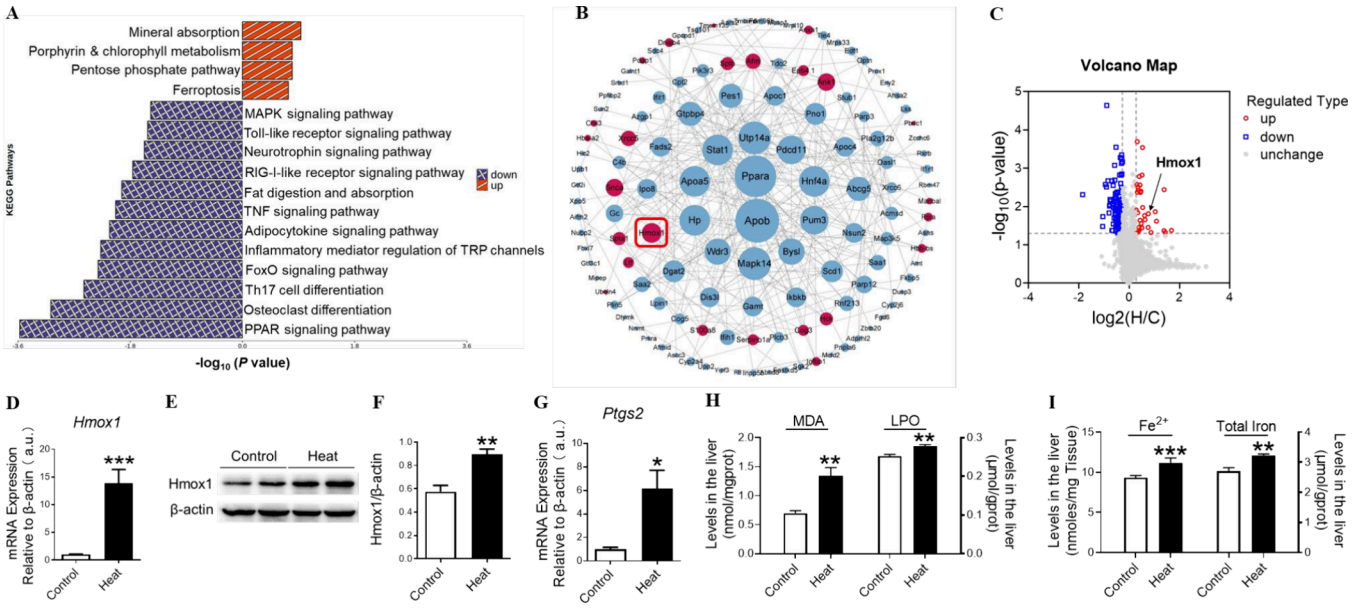

Figure 4. Ferroptosis in the liver of mice exposed to extreme heat mice were exposed to extreme heat until heatstroke onset and then allowed to recover at 22 °C for 9 h. A, KEGG signaling pathway analysis of proteomics with liver tissue (n = 3). B, Core protein network analysis of proteomics with liver tissue (n = 3). C, Volcano plot of proteomics with liver tissue (n = 3). D, The mRNA levels of *Hmox1* in the liver (n = 8). E,F, Representative bands (E) and analyzed protein levels of Hmox1 (F) in the liver (n = 4). G, qPCR analysis of *Ptgs2* in the liver (n = 8). H, MDA and LPO levels in the liver (n = 6). I, Fe^{2+} and total iron levels in the liver (n = 6). The numeric data are shown in Table S5. Data are presented as means ± SEM and assessed through t-test. *$p < 0.05$, **$p < 0.01$, ***$p < 0.001$, when compared with control group. Note: Hmox1, heme oxygenase 1; Ptgs2, prostaglandin-endoperoxide synthase 2; MDA, malondialdehyde; LPO, lipid peroxidation; SEM, standard error of the mean.

PPARα, PPARα Intervention and Liver Injury in Mice Exposed to Extreme Heat

To screen the potential target for extreme heat-induced liver injury, we performed proteomics analysis with liver tissues from mice following extreme heat exposure (Figure S2). KEGG analysis revealed that the PPAR signaling pathway was the most significantly dysregulated pathway, as indicated by the highest -$\log_{10}$(p-value) and the largest number of differentially expressed proteins (Figure 2A). Core protein network analysis identified PPARα as the central hub of the differentially expressed protein network (Figure 2B). Both mRNA (Figure 2D) and protein (Figure 2E,F) expression of PPARα were significantly downregulated in mice after being challenged with extreme heat.

To elucidate the role of PPARα in the extreme heat-induced liver injury, we first preadministered FF, a PPARα agonist, to the heatstroke mouse model (Figure S3A). FF treatment significantly mitigated extreme heat-induced Tc imbalance (Figure 3A), evidenced by continuously higher Tc and faster return to normal temperature than the extreme heat group during the recovery (Figure 3A and Figure S3B). FF preadministration exerted no attenuating effect on body weight decrease at Tc,max in response to extreme heat exposure (Figure S3C). Although the treatment significantly increased the liver weight (Figure S3D) and its organ coefficient (Figure S3E) in the control, it did not exert any effect in extreme heat-exposed mice. Interestingly, FF preadministration significantly ameliorated extreme heat-induced increases in ALT (Figure 3B) and AST (Figure 3C) levels, as well as the associated histological changes (Figure 3D) and Suzuki's score (Figure 3E). This was evidenced by less congestion, vacuole-like changes, and inflammatory infiltrates (Figure 3D).

Next, following the induction of heatstroke, mice received FF treatment to determine the therapeutic effects of PPARα intervention on extreme heat-induced liver injury. Consistent with the effects of preadministration, we observed that Tc in the T-HF group was significantly higher than in the T-HC group at 5 and 9 h during the recovery (Figure 3F). The elevation of ALT (Figure 3G) and AST (Figure 3H) levels in the heatstroke mice was significantly inhibited by the therapeutic FF treatment as well.

Then a mouse model of liver-specific overexpression of PPARα was induced to confirm the role of PPARα in extreme heat-induced heatstroke and liver injury. As shown in Figure 3I,J, hepatic PPARα expression was significantly higher in the overexpression group than in the AAV8 control group. Upon extreme heat exposure, the PPARα-overexpressed mice exhibited higher Tc at 2.5, 5, and 9 h during the recovery compared to the control (Figure 3K). Accordingly, the increased levels of ALT (Figure 3L) and AST (Figure 3M) were significantly mitigated by liver-specific PPARα overexpression.

Ferroptosis, Ferroptosis Inhibition and Liver Injury in Mice Exposed to Extreme Heat

Contrary to the downregulated PPAR signals, KEGG signaling pathway analysis revealed that mineral absorption, porphyrin, and chlorophyll metabolism, and ferroptosis signaling pathway were most significantly upregulated in response to extreme heat exposure, as indicated by the higher *-log10(p-value)* (Figure 4A). Core protein network analysis identified an upregulated molecule of Hmox1 as the central protein which was enriched in all three pathways (Figure 4B,C). Both mRNA (Figure 4D) and protein (Figure 4E,F) levels of hepatic Hmox1 were significantly elevated in mice after being challenged with extreme heat.

https://doi.org/10.1021/EHP.6c00267
Environ. Health Perspect. 2026, 134, 110−123

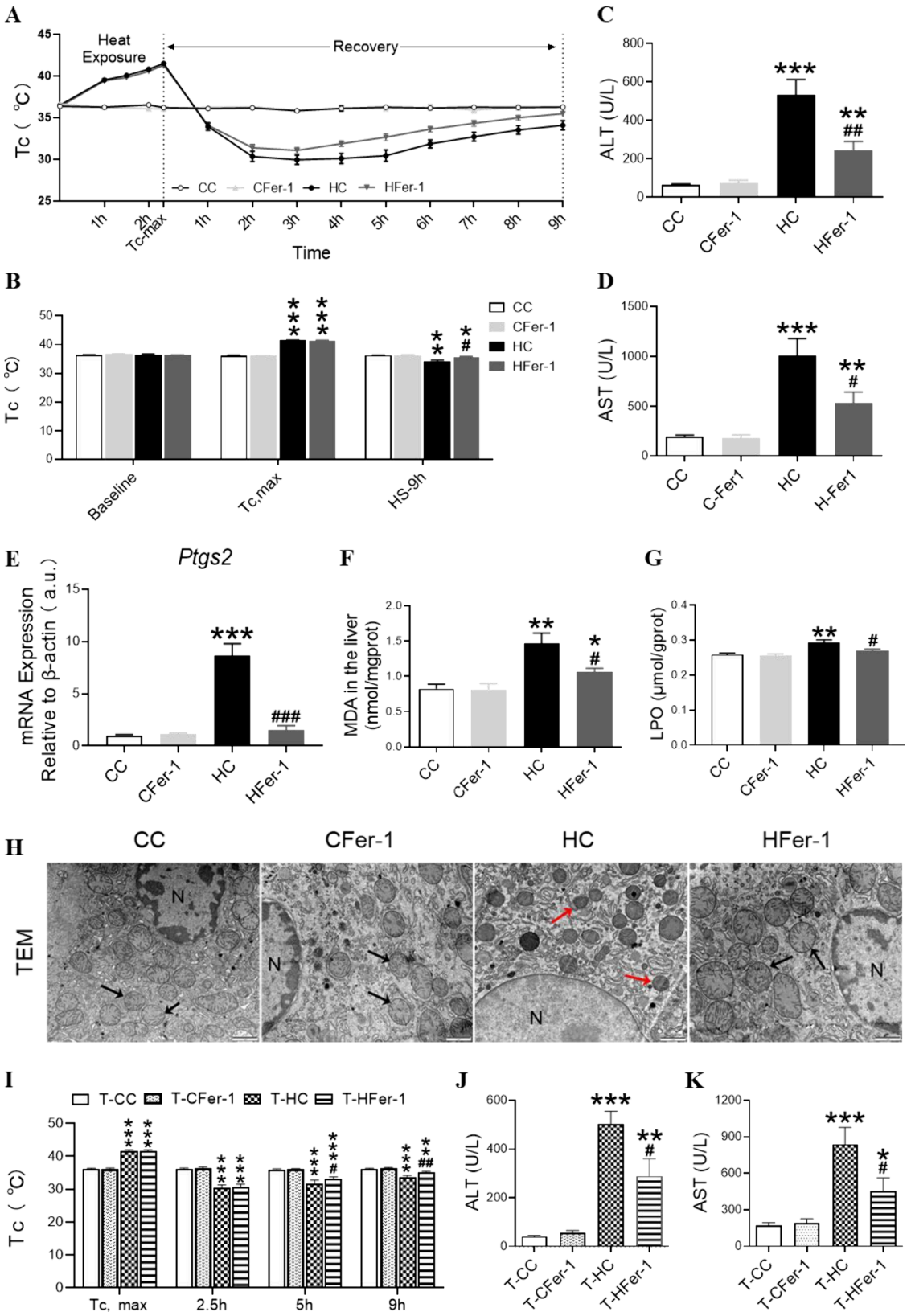

Figure 5. Effects of Fer-1 on Tc dysregulation and liver injury in mice exposed to extreme heat mice were treated with the ferroptosis inhibitor Fer-1 before/after heatstroke induction, followed by either a 9 h or a 24 h recovery period at 22 °C. A, The Tc during heat exposure and recovery period in the mice with Fer-1 preadministration (n = 8). B, Tc at baseline, Tc,max, HS-HD and HS-9h (n = 8). C,D, Serum ALT (C) and AST (D) levels at HS-9h (n = 8). E, qPCR analysis of *Ptgs2* in the liver (n = 8). F,G, MDA (F) and LPO (G) levels in the liver (n = 6). H, Representative images of transmission electron microscopy of the liver tissue. (black arrows indicate the normal mitochondrial structure; red arrows indicate the damaged mitochondrial structure) (n = 3). I, The Tc of mice during heat exposure and recovery period in the mice with Fer-1 therapeutic administration (n = 8). J,K, Serum ALT (J) and AST (K) levels at HS-24h (n = 8). The numeric data are shown in Table S6. Data are presented as

https://doi.org/10.1021/EHP.6c00267
Environ. Health Perspect. 2026, 134, 110−123

Figure 5. continued

means ± SEM and assessed through two-way ANOVA. *$p < 0.05$, **$p < 0.01$, ***$p < 0.001$, compared with CC group; $^{\#}p < 0.05$, $^{\#\#}p < 0.01$, $^{\#\#\#}p < 0.001$, compared with Fer-1 group. Note: ALT, alanine aminotransferase; AST, aspartate aminotransferase; Ptgs2, prostaglandin-endoperoxide synthase 2; MDA, malondialdehyde; LPO, lipid peroxidation; TEM, transmission electron microscope; SEM, standard error of the mean; ANOVA, analysis of variance.

Given the ability of Hmox1 to promote iron ion release, which initiates ferroptosis, we next examined the gold hallmarks to confirm the presence of ferroptosis. As shown in Figure 4G, extreme heat exposure significantly upregulated the levels of prostaglandin-endoperoxide synthase 2 (*Ptgs2*). Additionally, we observed an increase in lipid peroxidation markers, MDA and LPO (Figure 4H), as well as an increase in levels of Fe^{2+} and total iron (Figure 4I) in response to extreme heat.

To investigate the role of ferroptosis in extreme heat-induced liver injury, we first preadministered the mice with Fer-1, a ferroptosis inhibitor, before extreme heat exposure (Figure S4A). As shown in Figure 5A, the Fer-1 pretreatment group exhibited higher Tc than HC group during the recovery. Notably, at 9 h postheatstroke, Tc in the Fer-1 pretreatment group was markedly higher and closer to that of normal mice compared to the heatstroke group (Figure 5B). However, regardless of Fer-1 preadministration, body weight decreased at Tc,max after extreme heat exposure, whereas there was no difference in body weight among the groups at HS-9h (Figure S4B). Although liver weight (Figure S4C) and its organ coefficients (Figure S4D) remained unchanged either with or without Fer-1 pretreatment in extreme heat-exposed mice, Fer-1 pretreatment significantly mitigated the increased levels of circulating ALT (Figure 5C) and AST (Figure 5D) induced by extreme heat.

In addition, Fer-1 pretreatment reduced the elevation of ferroptosis markers, such as *ptgs2* (Figure 5E), MDA (Figure 5F) and LPO (Figure 5G). Furthermore, TEM examination showed that Fer-1 pretreatment alone exerted no alteration in mitochondrial structure compared to the control group. However, the hepatic mitochondria from extreme heat exposed mice exhibited smaller mitochondria and reduced or absent mitochondrial cristae, which was significantly ameliorated by Fer-1 pretreatment (Figure 5H).

Next, following the induction of heatstroke, mice received Fer-1 treatment to determine the therapeutic effects of ferroptosis inhibition on extreme heat-induced liver injury. Consistent with the effects of preadministration, we observed that Tc in the T-HFer-1 group was significantly higher than in the T-HC group at 5 and 9 h during the recovery (Figure 5I). The elevation of ALT (Figure 5J) and AST (Figure 5K) levels in the heatstroke mice was significantly inhibited by the therapeutic Fer-1 treatment as well.

PPARα, Ferroptosis and Liver Injury in Mice Exposed to Extreme Heat

To investigate whether the effects of PPARα activation on extreme heat-induced hepatic injury were via ferroptosis, we performed PPI analysis of all differentially expressed proteins regulated by PPARα. We found that PPARα negatively interacted with Hmox1 (Figure 6A), and the Co-IP assays indicated that these two proteins underwent a physical interaction (Figure 6B). Subsequently, we found that PPARα activation significantly inhibited levels of ferroptosis markers, including *Ptgs2* (Figure 6C), MDA (Figure 6D) and LPO

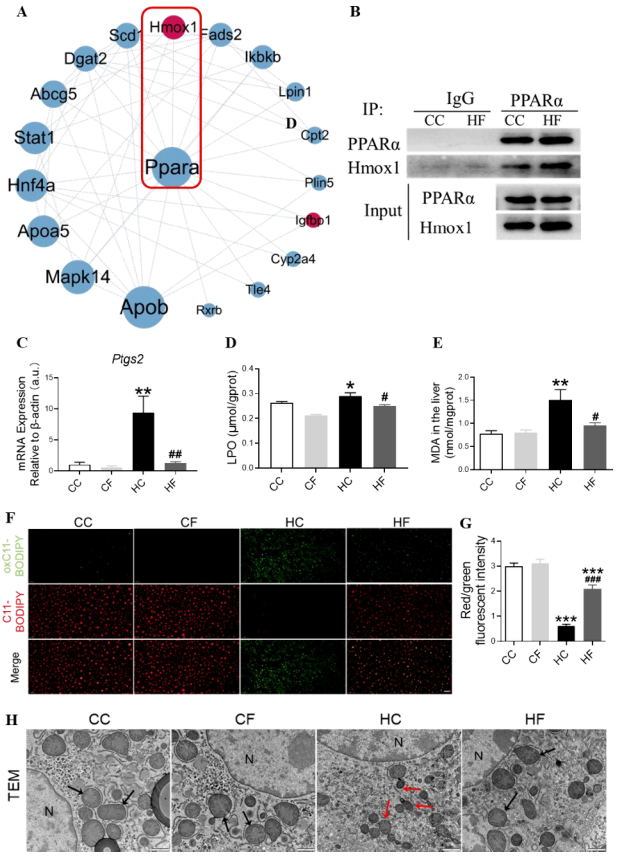

Figure 6. Effects of PPARα activation on ferroptosis in the liver of mice exposed to extreme heat mice received PPARα agonist fenofibrate intervention before heatstroke induction, followed by a 9 h recovery period at 22 °C. A, Protein−protein interaction analysis in the liver ($n = 3$). B, Co-IP of PPARα and Hmox1 in the liver. C, qPCR analysis of *Ptgs2* in the liver ($n = 8$). D−E, MDA (D) and LPO (E) levels in the liver ($n = 6$). F−G, Representative fluorescent images (F) and quantification of C11-BODIPY staining (G) of the liver section ($n = 5$). H, Representative images of transmission electron microscopy of the liver tissue. (black arrows indicate the normal mitochondrial structure; red arrows indicate the damaged mitochondrial structure) ($n = 3$). The numeric data are shown in Table S7. Data are presented as means ± SEM ($n = 3$−8) and assessed through two-way ANOVA. *$p < 0.05$, **$p < 0.01$, compared with CC group; $^{\#}p < 0.05$, $^{\#\#}p < 0.01$, compared with HC group. Note: PPARα, peroxisome proliferator-activated receptor α; Hmox1, Heme oxygenase 1; Ptgs2, prostaglandin-endoperoxide synthase 2; MDA, malondialdehyde; LPO, lipid peroxidation; Co-IP, Co-Immunoprecipitation; TEM, transmission electron microscope; SEM, standard error of the mean; ANOVA, analysis of variance.

(Figure 6E), which were all elevated in response to extreme heat exposure. To assess FF's impact on lipid peroxidation in vivo, the C11-BODIPY 581/591 probe was used. The heatstroke group showed a decreased red-to-green fluorescence ratio compared to that of the controls, which was partially blocked by PPARα activation (Figure 6F,G). In addition, PPARα activation significantly alleviated extreme

https://doi.org/10.1021/EHP.6c00267
Environ. Health Perspect. 2026, 134, 110−123

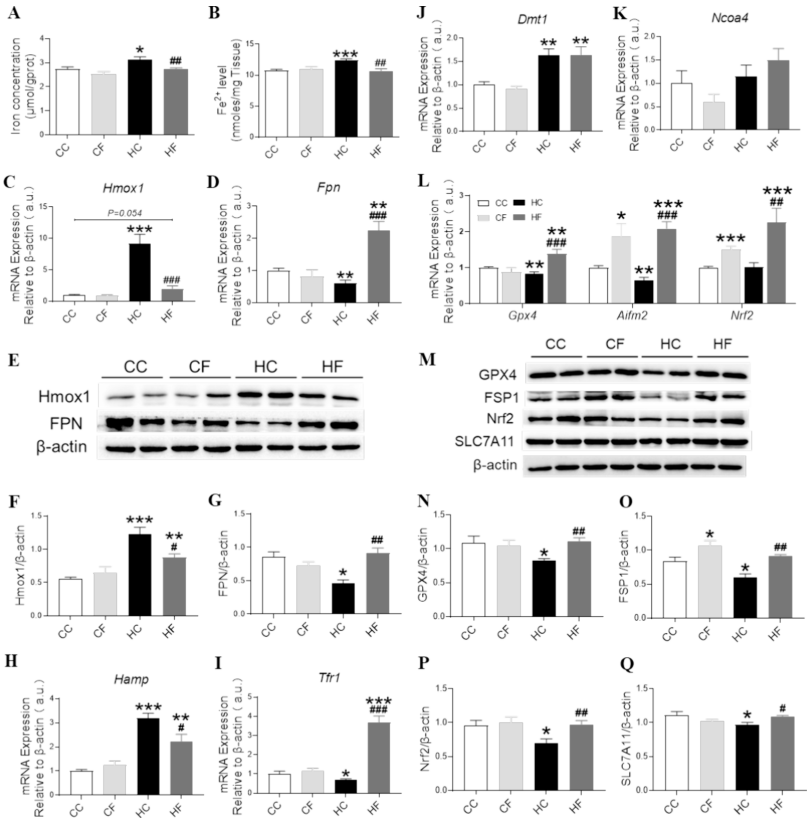

Figure 7. Molecular insights into the regulation of ferroptosis by PPARα activation mice received PPARα agonist fenofibrate intervention before heatstroke induction, followed by a 9 h recovery period at 22 °C. A,B, Total iron (A) and Fe^{2+} (B) levels in the liver ($n = 6$). C,D, qPCR analysis of *Hmox1* (C) and *Fpn* (D) in the liver ($n = 8$). E–G, Representative bands (E) and analyzed protein levels of Hmox1 (F) and FPN (G) in the liver ($n = 4$). H, qPCR analysis of *Hamp* in the liver ($n = 8$). I–K, qPCR analysis of *Tfr1* (I), *Dmt1* (J) and *Ncoa4* (K) in the liver ($n = 8$). L, qPCR analysis of *Gpx4*, *Aifm2* and *Nrf2* in the liver ($n = 8$). M–Q, Representative bands (M) and analyzed protein levels of GPX4 (N), FSP1 (O), Nrf2 (P) and SLC7A11 (Q) in the liver ($n = 4$). The numeric data are shown in Table S8. Data are presented as means ± SEM and assessed through two-way ANOVA. $^{*}p < 0.05$, $^{**}p < 0.01$, $^{***}p < 0.001$, compared with CC group; $^{\#}p < 0.05$, $^{\#\#}p < 0.01$, $^{\#\#\#}p < 0.001$, compared with HC group. Note: Hmox1, heme oxygenase 1; FPN, ferroportin; Tfr1, transferrin receptor 1; Dmt1, divalent metal transporter 1; Ncoa4, nuclear receptor coactivator 4; Aifm2, apoptosis-inducing factor, mitochondrial 2; GPX4, glutathione peroxidase 4; FSP1, ferroptosis suppressor protein 1; SLC7A11, solute carrier family 7, member 11; Nrf2, nuclear factor erythroid 2-related factor 2; SEM, standard error of the mean; ANOVA, analysis of variance.

heat-induced mitochondrial damage in the liver as well, as evidenced by the restoration of mitochondrial structure, including the normalization of mitochondrial size and reduced or absent mitochondrial cristae (Figure 6H).

PPARα and Ferroptosis: An Examination of Regulatory Mechanisms in Extreme Heat Scenarios

To elucidate the molecular mechanism by which PPARα activation suppressed ferroptosis induced by extreme heat exposure, we investigated ferroptosis-related signaling pathways. We first examined and observed that the elevated total iron (Figure 7A) and Fe^{2+} (Figure 7B) levels induced by extreme heat exposure were significantly attenuated by PPARα activation. Next, we investigated the levels of key molecules involved in iron metabolism. Extreme heat exposure significantly upregulated Hmox1 mRNA levels (Figure 7C) and downregulated FPN mRNA levels (Figure 7D), which were blocked and reversed by PPARα activation, respectively (Figure 7C,D). At the protein level, heat exposure increased Hmox1 (Figure 7E,F) and decreased FPN (Figure 7E,G) levels, which were partially and fully reversed by PPARα activation, as well. Similarly, PPARα activation partially mitigated the elevated *Hamp* mRNA levels observed in the liver of mice exposed to extreme heat (Figure 7H). In addition, extreme heat exposure decreased transferrin receptor 1 (*Tfr1*) mRNA (Figure 7I) whereas it increased divalent metal transporter 1 (*Dmt1*) mRNA levels (Figure 7J), with *Tfr1* being reversed by PPARα activation (Figure 7I). However, the mRNA levels of liver nuclear receptor coactivator 4 *(Ncoa4) were* not affected (Figure 7K).

To further clarify the mechanism of ferroptosis, we investigated the levels of key antioxidant enzymes involved in ferroptosis in the liver. Exposure to extreme heat significantly inhibited the mRNA levels of *Gpx4* and the apoptosis-inducing factor, mitochondrial 2 (*Aifm2*), which were blocked by PPARα activation (Figure 7L). Although extreme heat exposure did not affect *Nrf2* mRNA levels, PPARα activation significantly increased *Nrf2* mRNA expression (Figure 7L). Consistent with this, PPARα activation effectively blocked the decrease in protein levels of Gpx4 (Figure 7M,N), FSP1 (Figure 7M,O), Nrf2 (Figure 7M,P) and SLC7A11 (Figure 7M,Q).

DISCUSSION

Liver injury is a common complication of heatstroke and direct cause of death.[9] In this study, we have screened and identified the pivotal role of PPARα in extreme heat-induced liver injury,

https://doi.org/10.1021/EHP.6c00267
Environ. Health Perspect. 2026, 134, 110–123

which may be through ferroptosis-induced lipid peroxidation. We clearly demonstrated that PPARα expression was downregulated in the liver of mice subjected to heatstroke and liver injury and that either PPARα activation (both preventatively and therapeutically) or overexpression mitigated the severity of heatstroke-induced liver injury. Next, ferroptosis was induced in response to extreme heat exposure, and inhibition of ferroptosis alleviated heatstroke and associated liver injury in the mouse model. Finally, PPARα activation protected against extreme heat-induced liver injury by attenuating ferroptosis-induced lipid peroxidation, which may be achieved by restoring iron metabolism and enhancing the ferroptosis defense system (Figure 8).

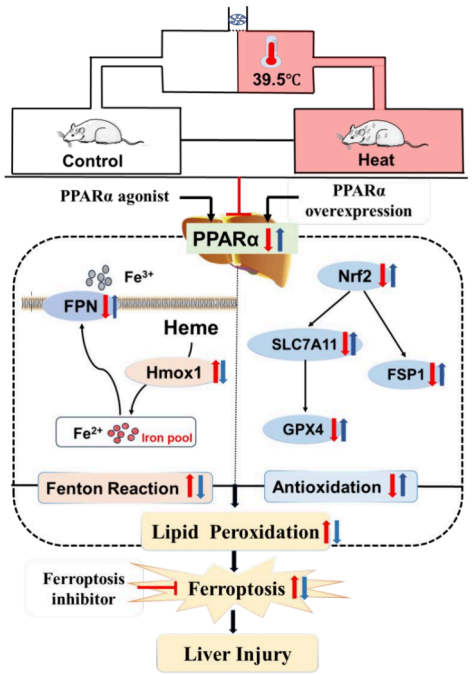

Figure 8. Hypothetical model for the role of PPARα in extreme heat-induced liver injury. The red arrow indicates hepatic changes in heatstroke mice. The blue arrow indicates effects of PPARα intervention in heatstroke mice. Note: PPARα, peroxisome proliferator-activated receptor α; FPN, ferroportin; GPX4, glutathione peroxidase 4; FSP1, ferroptosis suppressor protein 1; SLC7A11, solute carrier family 7, member 11; Nrf2, nuclear factor erythroid 2-related factor 2.

The first novelty of this study was that extreme heat-induced liver injury was mediated by PPARα. We successfully established a mouse model of heatstroke in which temperature disturbance and liver injury occurred early in HS-HD and continuously exacerbated at HS-9h. To elucidate the molecular mechanisms underlying extreme heat exposure-induced liver injury, proteomics analysis on liver tissues screened and identified PPARα as the most critically involved protein, with the PPAR signaling pathway being the most significantly perturbed one accordingly. To confirm the role of PPARα in extreme heat-induced liver injury, FF, an PPARα agonist, was utilized to observe the mitigated effects of PPARα activation on liver injury. As expected, both preventive and therapeutic administrations of FF significantly attenuated extreme heat-induced body temperature imbalance and liver injury. Furthermore, liver-specific PPARα overexpression in mice also conferred a similar protection. Thus, modulating PPARα activity, through agonists like FF, and enhancing PPARα expression offer promising strategies for both the prevention and treatment of heatstroke-induced liver injury.

The second finding was to identify ferroptosis as a key pathologic event in extreme heat-induced liver injury. Ferroptosis is a new form of regulated cell death characterized by iron-dependent lipid peroxidation.[22] The Fenton reaction was the central step in ferroptosis, in which Fe^{2+} catalyzes the oxidation of polyunsaturated fatty acids (PUFAs) in cell membranes, leading to the formation of toxic lipid peroxides that induce membrane rupture and cell death.[23] KEGG pathway analysis indicated that iron overload and ferroptosis may be involved in the pathogenesis of extreme heat-induced liver injury. To elucidate it, we administered ferroptosis inhibitor (Fer-1), both before and upon heatstroke, to mice and found that Fer-1 improved body temperature imbalance and liver injury on the basis of suppressing ferroptosis (as evidenced by inhibited expression of ferroptosis marker *Ptgs2*, decreased lipid peroxidation products MDA and LPO, and mitigated mitochondrial structure damage). These findings provide compelling evidence that ferroptosis is indeed involved in extreme heat-induced liver injury.

Mechanistically, we elucidated that PPARα activation exerted its protective effects on extreme heat-induced liver injury through the inhibition of ferroptosis. Bioinformatics analysis revealed that Hmox1, a key molecule in the ferroptosis pathway,[24] was the most significantly upregulated protein in the liver of mice exposed to extreme heat. Interestingly, protein−protein interaction analysis and Co-IP assay revealed that PPARα interacts with Hmox1, confirming the physical regulation of PPARα on ferroptosis regulation. Furthermore, we found that PPARα activation reduced the levels of ferroptosis markers involving Ptgs2, Fe^{2+}, MDA and LPO, and restored the mitochondrial structure in the liver of mice exposed to extreme heat, functionally indicating that PPARα activation did ameliorate hepatocyte ferroptosis caused by extreme heat exposure.

Iron homeostasis is a critical factor in ferroptosis, as iron overload can promote the Fenton reaction.[22] Fe^{2+} generation, efflux, and transportation are three biologic processes to maintain iron homeostasis. Hmox1 is the rate-limiting enzyme in heme catabolism by generating Fe^{2+}[24] and excessive Hmox1 expression could lead to the accumulation of intracellular Fe^{2+} and trigger ferroptosis.[25] In this study, we found that exposure to extreme heat significantly upregulated Hmox1 expression and iron levels, suggesting iron homeostasis dysregulation. Next, we examined the key proteins for iron efflux. Ferritin stores iron in hepatocytes, while FPN exports iron from hepatocytes to the blood.[26] Hepcidin (encoded by the *Hamp* gene), a peptide hormone produced by the liver, inhibits iron efflux by binding to FPN and promoting its degradation.[26] Our study found that extreme heat exposure upregulates *Hamp* expression and downregulates FPN levels in hepatocytes, explaining the accumulated intracellular Fe^{2+} and triggered ferroptosis. In addition, we examined molecules that regulate iron transportation. TFR1 is a transmembrane receptor on the cell membrane surface that can bind to Fe^{3+}-bound transferrin, enter the cell through endocytosis, and then be reduced to Fe^{2+} by lysosomal reductase.[22] DMT1 then transports Fe^{2+} to the lysosomal membrane and becomes part of the labile iron pool in the cytoplasm.[22] In this study, we found that exposure to extreme heat inhibited Tfr1 expression whereas it upregulated the level of Dmt1. Most of the extreme heat-dysregulated

https://doi.org/10.1021/EHP.6c00267
Environ. Health Perspect. 2026, 134, 110−123

expression of molecules for iron metabolism was partially or completely corrected by PPARα activation. Thus, it is deemed to say that PPARα activation could inhibit iron generation, promote iron efflux, and enhance iron uptake, thereby contributing to decreased iron burden and further suppressed ferroptosis in the extreme heat scenarios.

As long as ferroptosis occurs, cells are prone to evoke antioxidant systems localized in different subcellular compartments to counter toxic lipid peroxidation.[22] There were two pathways contributing to the process of countering lipid peroxidation during ferroptosis. The first one is Nrf2/SLC7A11-mediated GPX4 activation. GPX4 is a selenocysteine-dependent enzyme that neutralizes membrane phospholipid peroxides via glutathione (GSH), thereby suppressing lipid peroxidation.[27] GPX4 activity is inherently reliant on GSH bioavailability, which is tightly regulated by the Nrf2 through its control of cystine uptake.[28] Specifically, Nrf2 governs the expression of SLC7A11, the functional subunit of the cystine/glutamate antiporter system, which imports cystine—the rate-limiting precursor for GSH synthesis.[22] Another pathway that ferroptosis was suppressed was mediated by FSP1,[29] which utilized NAD(P)H to regenerate reduced coenzyme Q10 (CoQ10) and directly quenched lipid peroxyl radicals, offering a parallel antioxidant mechanism.[30] In this study, exposure to extreme heat markedly suppressed hepatic expression of GPX4, Nrf2, SLC7A11 and FSP1, collectively crippling both GSH-dependent and CoQ10-dependent antioxidant function. Notably, PPARα activation reversed the extreme heat-inhibited antioxidant system by restoring the expression of all four of the critical mediators. Thus, the enhancing effects of PPARα activation on the Nrf2-SLC7A11-GPX4 axis and FSP1/CoQ10 signaling underscored a synergistic strategy to counteract lipid peroxidation, ultimately alleviating extreme heat-induced hepatic ferroptosis.

In conclusion, our study delved into the complex mechanism of extreme heat-induced liver injury by identifying PPARα and PPARα-mediated ferroptosis. Notably, administration of PPARα agonist fenofibrate, a widely used medicine to improve dyslipidemia in clinic,[31] demonstrably ameliorated extreme heat-induced liver injury. Guided by the "old drug, new trick" paradigm, fenofibrate may be a promising clinical applicability for heatstroke treatment. These findings present novel insights into developing therapeutic interventions against heatstroke-associated liver injury.

■ ASSOCIATED CONTENT

Data Availability Statement

The mass spectrometry proteomics data have been deposited to the ProteomeXchange Consortium (https://proteomecentral.proteomexchange.org) via the iProX partner repository with the data set identifier PXD048585.

Supporting Information

The Supporting Information is available free of charge at https://pubs.acs.org/doi/10.1021/ehp.6c00267.

Figures of liver weight and its coefficient exposed to extreme heat, proteomics model, Effects of FF and Fer-1 on Tc, body weight, liver weight and its coefficient; tables of primers, summary data for Figures 1−7 in the main text (DOCX)

■ AUTHOR INFORMATION

Corresponding Author

Cuiqing Liu − *School of Public Health, Zhejiang Chinese Medical University, Hangzhou, Zhejiang 310053, China; Zhejiang International Science and Technology Cooperation Base of Air Pollution and Health, Hangzhou, Zhejiang 310053, China; First Affiliated Hospital of Zhejiang Chinese Medical University, Hangzhou 310053, China;* orcid.org/0000-0002-0393-7806; Email: liucuiqing@zcmu.edu.cn

Authors

Guoqing Zhang − *School of Public Health, Zhejiang Chinese Medical University, Hangzhou, Zhejiang 310053, China; Department of Clinical Nutrition, West China Hospital of Sichuan University, Chengdu 610093, China*

Lisha Zhao − *School of Public Health, Zhejiang Chinese Medical University, Hangzhou, Zhejiang 310053, China; Zhejiang International Science and Technology Cooperation Base of Air Pollution and Health, Hangzhou, Zhejiang 310053, China*

Jiahui Wang − *School of Public Health, Zhejiang Chinese Medical University, Hangzhou, Zhejiang 310053, China*

Kunyi Wang − *School of Public Health, Zhejiang Chinese Medical University, Hangzhou, Zhejiang 310053, China*

Xiuyu Ji − *Departments of Pathology and Pathophysiology and Cardiology, Second Affiliated Hospital, Zhejiang University School of Medicine, Hangzhou, Zhejiang 310058, China; Key Laboratory of Disease Proteomics of Zhejiang Province, Zhejiang University School of Medicine, Hangzhou, Zhejiang 310058, China*

Renjie Hu − *School of Public Health, Zhejiang Chinese Medical University, Hangzhou, Zhejiang 310053, China; Zhejiang International Science and Technology Cooperation Base of Air Pollution and Health, Hangzhou, Zhejiang 310053, China*

Tong Hou − *School of Public Health, Zhejiang Chinese Medical University, Hangzhou, Zhejiang 310053, China; Zhejiang International Science and Technology Cooperation Base of Air Pollution and Health, Hangzhou, Zhejiang 310053, China*

Lu Zhang − *School of Public Health, Zhejiang Chinese Medical University, Hangzhou, Zhejiang 310053, China; Zhejiang International Science and Technology Cooperation Base of Air Pollution and Health, Hangzhou, Zhejiang 310053, China*

Ran Li − *School of Public Health, Zhejiang Chinese Medical University, Hangzhou, Zhejiang 310053, China; Zhejiang International Science and Technology Cooperation Base of Air Pollution and Health, Hangzhou, Zhejiang 310053, China;* orcid.org/0000-0002-6268-8811

Qinghua Sun − *School of Public Health, Zhejiang Chinese Medical University, Hangzhou, Zhejiang 310053, China; Zhejiang International Science and Technology Cooperation Base of Air Pollution and Health, Hangzhou, Zhejiang 310053, China*

Kezhong Zhang − *Center for Molecular Medicine and Genetics, Wayne State University School of Medicine, Detroit, Michigan 48201, United States*

Complete contact information is available at: https://pubs.acs.org/10.1021/EHP.6c00267

https://doi.org/10.1021/EHP.6c00267
Environ. Health Perspect. 2026, 134, 110−123

Notes

The authors declare no competing financial interest.

■ ACKNOWLEDGMENTS

We would like to express our sincere gratitude to Professor Zhuoxian Meng for his invaluable guidance and support throughout the experiment. Special thanks are also due to Yidan Wang for her technical assistance in experimental execution. This work was supported by National Natural Science Foundation of China (grant number 82173480, 81973001 and 82273590), Sichuan Science and Technology Program (grant number 2025ZNSFSC1550), and "Qimingxing" Research Fund for Young Talents of West China Hospital (No. HXQMX0096).

■ REFERENCES

(1) Wang, Y. J.; Wang, A. Q.; Zhai, J. Q.; Tao, H.; Jiang, T.; Su, B. D. Tens of thousands additional deaths annually in cities of China between 1.5 degrees C and 2.0 degrees C warming. *Nat. Commun.* **2019**, *10*, 3376.

(2) Watts, N.; Amann, M.; Arnell, N.; Ayeb-Karlsson, S.; Beagley, J.; Belesova, K.; et al. The 2020 report of The Lancet Countdown on health and climate change: responding to converging crises. *Lancet* **2021**, *397* (10269), 129−170 PMID:33278353.

(3) Ebi, K. L.; Capon, A.; Berry, P.; Broderick, C.; de Dear, R.; Havenith, G.; et al. Hot weather and heat extremes: health risks. *Lancet* **2021**, *398* (10301), 698−708 PMID:34419205.

(4) Faurie, C.; Varghese, B. M.; Liu, J.; Bi, P. Association between high temperature and heatwaves with heat-related illnesses: A systematic review and meta-analysis. *Sci. Total Environ.* **2022**, *852*, 158332 PMID:36041616.

(5) Barriopedro, D.; Fischer, E. M.; Luterbacher, J.; Trigo, R. M.; Garcia-Herrera, R. The hot summer of 2010: redrawing the temperature record map of Europe. *Science* **2011**, *332* (6026), 220−4 PMID:21415316.

(6) Sun, X.; Sun, Q.; Zhou, X.; Li, X.; Yang, M.; Yu, A.; et al. Heat wave impact on mortality in Pudong New Area, China in 2013. *Sci. Total Environ.* **2014**, *493*, 789−94 PMID:25000574.

(7) Tobías, A.; Madaniyazi, L.; Gasparrini, A.; Armstrong, B. High Summer Temperatures and Heat Stroke Mortality in Spain. *Epidemiology* **2023**, *34* (6), 892−896 PMID:WOS:001076032000019.

(8) Bouchama, A.; Abuyassin, B.; Lehe, C.; Laitano, O.; Jay, O.; O'Connor, F. G.; et al. Classic and exertional heatstroke. *Nat. Rev. Dis Primers* **2022**, *8* (1), 8 PMID:35115565.

(9) Wang, F.; Zhang, Y.; Li, J.; Xia, H.; Zhang, D.; Yao, S. The pathogenesis and therapeutic strategies of heat stroke-induced liver injury. *Crit Care* **2022**, *26* (1), 391 PMID:36528615.

(10) Fan, S.; Gao, Y.; Qu, A.; Jiang, Y.; Li, H.; Xie, G.; et al. YAP-TEAD mediates PPAR alpha-induced hepatomegaly and liver regeneration in mice. *Hepatology* **2022**, *75* (1), 74−88 PMID:34387904.

(11) Zhong, J.; He, X. F.; Gao, X. X.; Liu, Q. H.; Zhao, Y.; Hong, Y. Hyodeoxycholic acid ameliorates nonalcoholic fatty liver disease by inhibiting RAN-mediated PPARa nucleus-cytoplasm shuttling. *Nat. Commun.* **2023**, *14* (1), 5451.

(12) Paumelle, R.; Haas, J. T.; Hennuyer, N.; Bauge, E.; Deleye, Y.; Mesotten, D.; et al. Hepatic PPARalpha is critical in the metabolic adaptation to sepsis. *J. Hepatol* **2019**, *70* (5), 963−973 PMID:30677458.

(13) Lim, C. L. Heat Sepsis Precedes Heat Toxicity in the Pathophysiology of Heat Stroke-A New Paradigm on an Ancient Disease. *Antioxidants (Basel)* **2018**, *7* (11), 149.

(14) Fang, X.; Ardehali, H.; Min, J.; Wang, F. The molecular and metabolic landscape of iron and ferroptosis in cardiovascular disease. *Nat. Rev. Cardiol* **2023**, *20* (1), 7−23 PMID:35788564.

(15) Dixon, S. J.; Pratt, D. A. Perspective Ferroptosis: A flexible constellation of related biochemical mechanisms. *Mol. Cell* **2023**, *83* (7), 1030−1042 PMID:WOS:000975943300001.

(16) Hou, Y.; Wang, X.; Ping, J.; Lei, Z.; Gao, Y.; Ma, Z.; et al. Metabonomics Approach to Assessing the Modulatory Effects of Kisspeptin-10 on Liver Injury Induced by Heat Stress in Rats. *Sci. Rep* **2017**, *7* (1), 7020 PMID:28765538.

(17) Das, A. Heat stress-induced hepatotoxicity and its prevention by resveratrol in rats. *Toxicol Mech Methods* **2011**, *21* (5), 393−9 PMID:21426263.

(18) Wickham, K. A.; Wallace, P. J.; Cheung, S. S. Sex differences in the physiological adaptations to heat acclimation: a state-of-the-art review. *Eur. J. Appl. Physiol* **2021**, *121* (2), 353−367 PMID:33205218.

(19) Li, R.; Wang, Y.; Hou, B.; Lam, S. M.; Zhang, W.; Chen, R.; et al. Lipidomics insight into chronic exposure to ambient air pollution in mice. *Environ. Pollut.* **2020**, *262*, 114668 PMID:32443199.

(20) He, S.; Li, R.; Peng, Y.; Wang, Z.; Huang, J.; Meng, H.; et al. ACSL4 contributes to ferroptosis-mediated rhabdomyolysis in exertional heat stroke. *J. Cachexia Sarcopenia Muscle* **2022**, *13* (3), 1717−1730.

(21) Lefere, S.; Puengel, T.; Hundertmark, J.; Penners, C.; Frank, A. K.; Guillot, A.; et al. Differential effects of selective- and pan-PPAR agonists on experimental steatohepatitis and hepatic macrophages(☆). *J. Hepatol* **2020**, *73* (4), 757−770 PMID:32360434.

(22) Chen, J.; Li, X.; Ge, C.; Min, J.; Wang, F. The multifaceted role of ferroptosis in liver disease. *Cell Death Differ.* **2022**, *29* (3), 467−480 PMID:35075250.

(23) He, Y. J.; Liu, X. Y.; Xing, L.; Wan, X.; Chang, X.; Jiang, H. L. Fenton reaction-independent ferroptosis therapy via glutathione and iron redox couple sequentially triggered lipid peroxide generator. *Biomaterials* **2020**, *241*, 119911 PMID:32143060.

(24) Menon, A. V.; Liu, J.; Tsai, H. P.; Zeng, L.; Yang, S.; Asnani, A.; et al. Excess heme upregulates heme oxygenase 1 and promotes cardiac ferroptosis in mice with sickle cell disease. *Blood* **2022**, *139* (6), 936−941 PMID:34388243.

(25) Fang, X.; Wang, H.; Han, D.; Xie, E.; Yang, X.; Wei, J.; et al. Ferroptosis as a target for protection against cardiomyopathy. *Proc. Natl. Acad. Sci. U. S. A.* **2019**, *116* (7), 2672−2680 PMID:30692261.

(26) Sagar, P.; Angmo, S.; Sandhir, R.; Rishi, V.; Yadav, H.; Singhal, N. K. Effect of hepcidin antagonists on anemia during inflammatory disorders. *Pharmacol Ther* **2021**, *226*, 107877 PMID:33895185.

(27) Liu, Y.; Wan, Y.; Jiang, Y.; Zhang, L.; Cheng, W. GPX4: The hub of lipid oxidation, ferroptosis, disease and treatment. *Biochim Biophys Acta Rev. Cancer* **2023**, *1878* (3), 188890.

(28) Wang, Y. L.; Yan, S.; Liu, X. M.; Deng, F.; Wang, P. C.; Yang, L. Y.; et al. PRMT4 promotes ferroptosis to aggravate doxorubicin-induced cardiomyopathy via inhibition of the Nrf2/GPX4 pathway. *Cell Death and Differentiation* **2022**, *29* (10), 1982−1995 PMID:WOS:000779772400002.

(29) Jiang, X.; Stockwell, B. R.; Conrad, M. Ferroptosis: mechanisms, biology and role in disease. *Nat. Rev. Mol. Cell Biol.* **2021**, *22* (4), 266−282.

(30) Bersuker, K.; Hendricks, J. M.; Li, Z.; Magtanong, L.; Ford, B.; Tang, P. H.; et al. The CoQ oxidoreductase FSP1 acts parallel to GPX4 to inhibit ferroptosis. *Nature* **2019**, *575* (7784), 688−692 PMID:31634900.

(31) McKeage, K.; Keating, G. M. Fenofibrate A Review of its Use in Dyslipidaemia. *Drugs* **2011**, *71* (14), 1917−1946 PMID:-WOS:000296069300008.